CHEMISTRY
A EUROPEAN JOURNAL

DOI: 10.1002/chem.201001938

Comparing the Enantioselective Power of Steric and Electrostatic Effects in Transition-Metal-Catalyzed Asymmetric Synthesis

Albert Poater,[a, b] Francesco Ragone,[a] Ronaldo Mariz,[c] Reto Dorta,*[c] and Luigi Cavallo*[a]

Abstract: The current approach to improve and tune the enantioselective performances of transition-metal catalysts for asymmetric synthesis is mostly focused to modifications of the steric properties of the ancillary ligands of the active metal. Nevertheless, it is also known that electrostatic effects can have a remarkable role to promote selectivity in asymmetric synthesis. Using the Rh-catalyzed asymmetric 1,4-addition of phenylboronic acid to 2-cyclohexenone leading to chiral 3-phenylcyclohexanone as an example, we could show that high enantioselectivity can be indeed achieved using catalysts essentially based either on steric or electrostatic effects as the main source of enantioselective induction. In this contribution we suggest that the analysis of the surface of interaction between the catalyst and the substrate could be a useful tool to quantify the power of steric and electrostatic effects of catalysts.

Keywords: asymmetric catalysis · enantioselectivity · homogeneous catalysis · rhodium

Introduction

Asymmetric synthesis is at the heart of industrial chemistry and enzymatic processes in nature, with prochiral C=C double bonds as one of the substrates of excellence. Focusing on industrial applications, asymmetric processes involving prochiral olefins span from the synthesis of commodities, such as stereoregular polymers,[1–2] to the synthesis of specialty products in the pharmaceutical industry,[3–4] with an economic impact difficult to quantify (the market for stereoregular polymers alone is in the order of 10^{10} USD per year). Among the most common elementary steps in these fields are two fundamental reactions, namely asymmetric C–C bond formation and hydrogenation,[3–8] and any general advance in the development of new strategies for the design of better performing catalysts for these reactions can have scientific and technical consequences that cannot be easily estimated.

By definition, successful asymmetric synthesis involving prochiral substrates is based on the ability of a chiral catalyst to promote preferential reactivity along one of the diastereoselective reaction pathways leading to the two enantiomeric products at the end of the reaction.[9–10] To induce a catalyst to transfer the chiral information stored in its chiral structure to the substrates in the enantioselective step, steric and electronic effects are the standard tools for chemists. However, while it is well accepted that nature uses both these effects to promote (pro)chiral recognition,[11–12] the development of synthetic catalysts based on transition-metal complexes is clearly more confined to use the steric handle. Among the few and noticeable examples in catalysis in which electronic effects are suggested to play a role is the Sharpless epoxidation, but even in such a system steric interactions between reactants and coordinated ligands seem to play a determining role.[13–15] The reason for this preference for steric effects probably arises from the simple fact that early examples of privileged ligands for asymmetric metal catalysis can be more readily and systematically modified using sterically different substituents. Increasing the size of an alkyl substituent as in the Me, Et, *i*Pr and *t*Bu series or substituting phenyl groups in *ortho*, *meta* or *para* positions

[a] Dr. A. Poater, Dr. F. Ragone, Prof. Dr. L. Cavallo
Department of Chemistry, University of Salerno
Via Ponte don Melillo, 84084 Fisciano (Italy)
Fax: (+39) 089-969603
E-mail: lcavallo@unisa.it

[b] Dr. A. Poater
Catalan Institute for Water Research (ICRA)
H2O Building, Scientific and
Technological Park of the University of Girona
Emili Grahit 101, 17003 Girona (Spain)

[c] Dr. R. Mariz, Prof. Dr. R. Dorta
Institute of Organic Chemistry, University of Zürich
Winterthurerstrasse 190, 8057 Zürich (Switzerland)
E-mail: dorta@oci.uzh.ch

Supporting information for this article is available on the WWW under http://dx.doi.org/10.1002/chem.201001938.

with additional alkyl/aryl groups are the most classical examples.

This historical preference for modulating steric effects as the main strategy in the development of new transition-metal catalysts for asymmetric synthesis has confined electrostatic effects to a less relevant role. Nevertheless, new Rh catalysts developed recently for the 1,4-addition of phenylboronic acid to 2-cyclohexenone leading to chiral 3-phenylcyclohexanone with remarkably high enantioselectivity (see below)[16–19] is among those examples that indicate that steric and electronic effects might be used interchangeably within structurally closely related ligand–metal systems (in both L-**1** and L-**2** the catalyst is a square-planar Rh complex). We show here that this is indeed the case, which we believe reinforces the idea that more efforts should be directed towards using electrostatic effects more systematically in the development of metal catalysts for asymmetric synthesis. Further, we propose that the analysis of the interaction surface between the catalyst and the substrate can be a powerful tool to analyze and rationalize the steric and electrostatic properties of a catalyst even without the computational analysis of the whole reaction pathway. This approach could be an extremely powerful tool to screen rapidly new catalysts to steer experimental efforts towards the most promising solutions. We have already introduced topographic steric maps to characterize Ru complexes relevant to olefin metathesis, and to support the proposed mechanism for asymmetric ring-closing metathesis promoted by the same complexes.[20–21] As a final remark, we clarify that the two effects we analyze in this work do not exclude each other. Rather, both of them are present but with different intensity in the different catalysts.

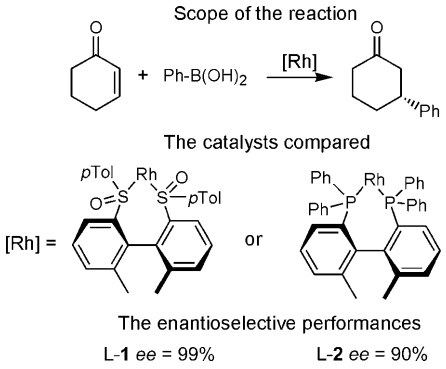

Back to the reaction shown above, which is the reaction investigated in this paper, for the sake of simplicity, we focus on the C–C bond formation step starting from the [Rh]-phenyl species, which is the enantioselective step.

Computational Details

DFT calculations: All DFT static calculations were performed at the GGA level with the Gaussian03 set of programs,[22] using the BP86 functional of Becke and Perdew.[23–26] The electronic configuration of the molecular systems was described with the standard split-valence basis set with a polarization function of Ahlrichs and co-workers for H, C, N, O, P, F, and Cl (SVP keyword in Gaussian).[26] For Rh we used the small-core, quasi-relativistic Stuttgart/Dresden effective core potential, with an associated (8s7p6d)/[6s5p3d] valence basis set contracted according to a (311111/22111/411) scheme (standard SDD keywords in Gaussian). The geometry optimizations were performed without symmetry constraints, and the characterization of the located stationary points was performed by analytical frequency calculations. The energies discussed throughout the text contain zero point energy corrections. Solvent effects including contributions of non electrostatic terms have been estimated in single point calculations on the gas-phase optimized structures, based on the polarizable continuous solvation model PCM to simulate the toluene/H_2O (10:1) mixture as a solvent.[27]

Topographic steric maps: The steric maps have been calculated for one unit of the dimeric [L-**1**RhCl]$_2$ and [L-**2**RhCl]$_2$ precursors of L-**1** and L-**2** optimized under a C_2-symmetry constraint. The points in space defining the steric map were located with the Samb*V*ca package developed by us.[28] This program analyzes the first coordination sphere around the metal, which is the place where catalysis occurs. It is normally used to calculate the buried volume of a given ligand, which is a number that quantifies the amount of the first coordination sphere of the metal occupied by this ligand.[29–34] We modified Samb*V*ca to understand how the ligand is distributed around the metal, which is the shape of the reactive pocket. We already introduced topographic steric maps to characterize Ru-complexes relevant to olefin metathesis.[21]

To build the steric map, the Rh unit under analysis has been placed with the Rh center at the origin, with the C_2-symmetry axis aligned along the z axis, and with the Cl atoms in the yz plane at positive z values. After this alignment step the Cl atoms have been removed (because they do not belong to the L-**1** and L-**2** ligands) and the first coordination sphere around the metal is analyzed. This sphere, of radius R, is sectioned by a regular 3D cubic mesh of spacing s, which defines cubic voxels v. The distance between the center of each voxel with all the atoms in the ligand is tested to check if any of the atoms is within a van der Waals distance from the centre of the examined voxel. If no atom is within a van der Waals distance, the examined voxel is marked as a free voxel. Otherwise, the examined voxel is marked as buried.

After all the voxels in the first coordination sphere have been marked as free or buried, for each (x,y) point within the first coordination sphere the program scans the sphere from the top (i.e., away from the ligand) to find at which z value there is the first buried voxel. This procedure results in a surface, defined as $S(x,y)=z_B$, which represents the surface of the ligand that is exposed towards the incoming reactants. In other words, this $S(x,y)=z_B$ surface defines the shape of the reactive pocket. Positive values of z_B indicate that the ligands protrudes in the $z>0$ half-sphere, which is the half-sphere where the reacting groups are placed. A schematic representation of the interaction surface between the catalyst and the substrate is shown in Figure 1.

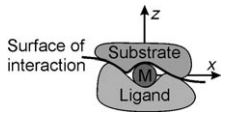

Figure 1. Schematic representation of the interaction surface between the substrate and the catalyst.

Finally, the maps are a simple 2D isocontour representation of the interaction surface $S(x,y)=z_B$. In this work, the radius R of the sphere around the metal center was set to 3.5 Å, while for the atoms we adopted the Bondi radii[35] scaled by 1.17, and a mesh of 0.1 Å was used to scan the sphere for buried voxels.

Topographic electrostatic maps: The interaction surface $S(x,y)=z_B$ defined above was characterized in terms of the electrostatic potential. For these calculations the whole dimeric [L-**1**RhCl]$_2$ and [L-**2**RhCl]$_2$ precursors had to be used to preserve the electroneutrality and the C_2 symmetry of the system. Since the points $S(x,y)=z_B$ are at the surface of one of the Rh units, the electrostatic potential at these points will be dominated by atoms belonging to the same Rh unit used to define the interaction sur-

face *S*. Thus, with the Gaussian03 program and with the density functional and basis set described above we calculated the electrostatic potential at the *xyz* points defining the interaction surface $S(x,y)=z_B$. The topographic electrostatic maps simply report isopotential curves.

Since the main scope of this work is to analyze the reactive pocket casted by the L-**1** and L-**2** ligands around the catalytically active Rh center, and that the same shape can be obtained with steric effects in one case and electrostatic in the other, we decided to calculated the topographic maps in the absence of the Rh–Ph bond or the incoming alkene. We believe this analysis is more general, since it has been performed on the precatalyst, and thus describes intrinsic properties of the catalyst and can be applied to any reaction when the same ligands are wrapped around the metal. Of course, the final shape of the reactive pocket will depend on the contribution of the Rh–Ph bond as well, but we believe this contribution will add as a perturbation to the basic shape casted by the ligand. For this reason, we did not try to make a quantitative correlation between the topographic maps and the experimental selectivity.

Results and Discussion

Energy analysis of the reaction pathways: The reaction pathways from the L-Rh-phenyl species are reported in Figure 2 for both L-**1** and L-**2**. Different from the well-established model put forth early on by Hayashi et al., the initial coordination of the olefin onto the L-Rh–phenyl species, structures **A** in Figure 2, marginally discriminates between the pro-*R* and pro-*S* face approaches of the olefin, regardless of whether L-**1** and L-**2** is used,[36] and actually for L-**1** the pro-*S* face is even slightly favored. Rather, the energetic profiles of Figure 1 clearly show that the rate-determining and enantioselective step corresponds to the C–C bond formation step, in which the C=C bond of 2-cyclohexen-1-one inserts into the Rh–Ph bond. For this reason, in the following we will focus mainly on transition state **A**–**B**, corresponding to the C–C bond formation. For both L-**1** and L-**2** the transition state **A**–**B** leading to the *S* product is higher in energy than that leading to the *R* product, which is in agreement with the experimentally observed preferential formation of the *R* product when L catalysts are used.[17–18] Further, the energy difference between the competing transition states pro-*S* and pro-*R*, 4.4 and 6.1 kcal mol^{-1} for L-**1** and L-**2**, respectively, is quite high and at the end rather similar, which is in agreement with the similarly high enantioselectivity shown by these catalysts.[17–18]

Overall, the L-**1** and L-**2** energetic profiles are very similar. In both cases the energy barrier for the pro-*R* C–C formation step is roughly 11–13 kcal mol^{-1}, water coordination to intermediate **C** results in an energy gain of 10 kcal mol^{-1} roughly, and the resulting water coordination intermediate **D** is roughly 25–30 kcal mol^{-1} below the starting coordination intermediate **A**, the barrier for the proton transfer step (the NPA charge on the transferred H atom in transition state **D**–**E** is +0.50e and +0.42e for L-**1** and L-**2**, respectively, which indicates this as a proton transfer step) is roughly 5 kcal mol^{-1}, and the final geometry corresponding to the coordinated product **E** is roughly 28–29 kcal mol^{-1} below the starting coordination intermediate **A**. This indicates that the rather different nature of the Rh ligand does not influence

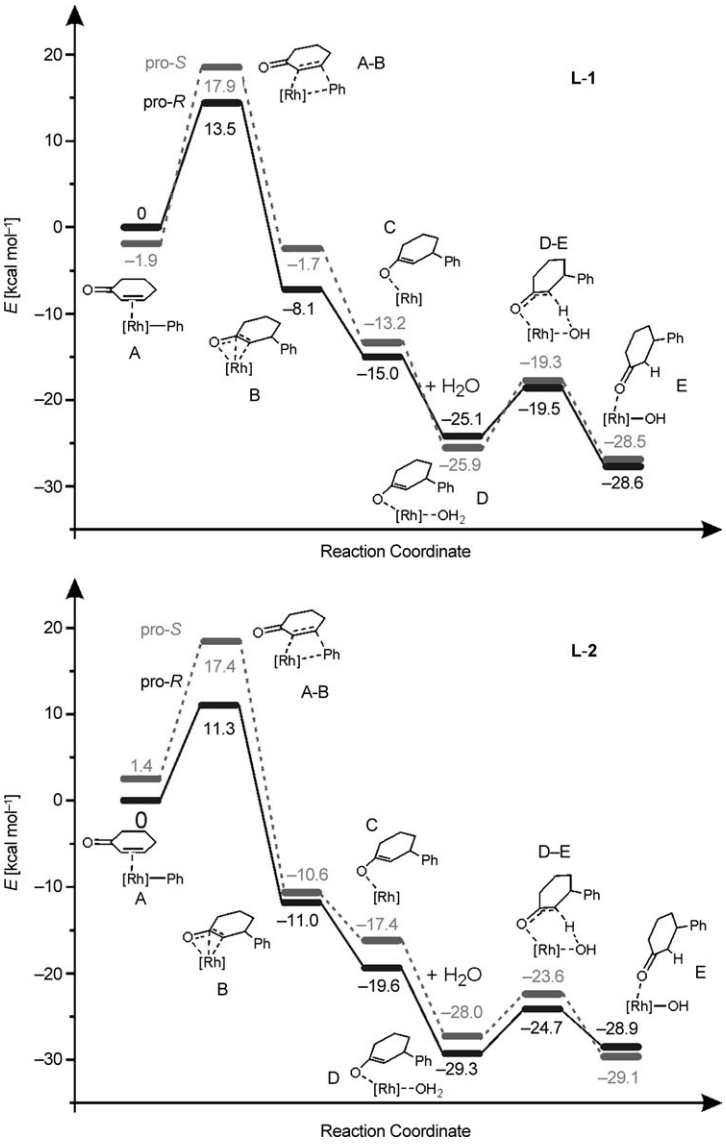

Figure 2. Reaction profiles for the C–C bond formation step with L-**1** (top) and L-**2** (bottom).

in a dramatic way the course of the reaction, which is not an obvious and predictable conclusion.

Nevertheless, the main scope of this work is not to enter into the fine details of the structures and the energetics along the reaction pathways, but rather to focus on something that we believe is more important, which is the source of enantioselectivity in the two catalysts. For this reason we move immediately to the enantioselective step without further discussing the reaction pathways of Figure 2.

Focusing on the enantioselective C–C bond formation step, the analysis of the geometries of the key transition state, shown in Figure 3, indicate that the most favored pro-*R* transition state of L-**1** presents both the Ph and the C=O groups of the substrate in rather open parts of space, which is on the side of the *p*-tolyl rings that are bent away (down) from the Rh atom. The competitive pro-*S* transition state,

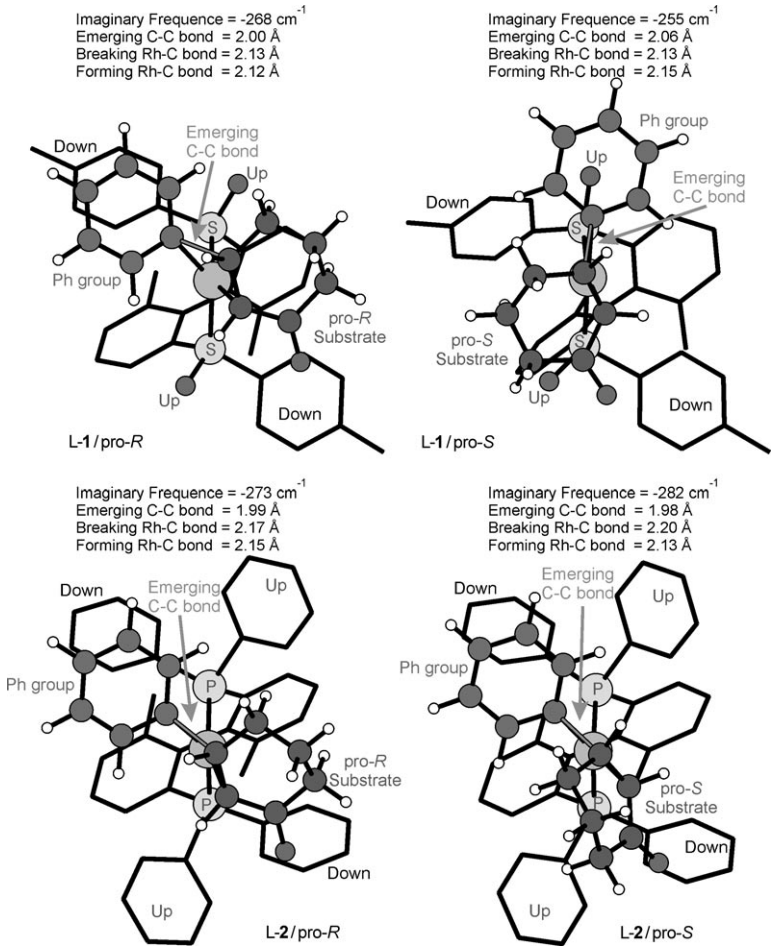

Figure 3. Transition states for the favored pro-*R* and unfavored pro-*S* C–C bond formation step with L-**1** (top) and L-**2** (bottom).

instead, is disfavored by repulsive steric/electrostatic interactions between both the Ph group and the C=O group of the substrate with the pointing up S=O groups of the ligand. Moving to the transition states pro-*R* and pro-*S* of L-**2**, it is clear that the disposition of the Ph group and of the 2-cyclohexen-1-one is very similar to that in the corresponding pro-*R* and pro-*S* transition states of L-**1**. However, for L-**2** the reacting groups have to avoid the phenyl groups of the Rh ligand that point up, that is, towards them. This indicates that the S=O groups in L-**1** and the pointing up phenyl groups in L-**2** have the same enantioselective role. Of course, the origin of enantioselectivity is electrostatic in L-**1** and steric in L-**2**, but this conclusion cannot emerge from the analysis discussed so far, which only indicates that there is some energy difference in the C–C bond formation step with both catalysts.

Topographic steric and electrostatic maps: To clarify which forces are at the origin of the enantioselective effect in L-**1** and L-**2** we analyzed the first coordination sphere of the Rh in L-**1** and L-**2**, where the catalytic action takes place, in terms of steric and electrostatic effects using topographic maps (see Figure 4). These topographic maps characterize the surface that the ligands offer to the substrate, and their properties define the catalyst–substrate interaction, thus allowing to illuminate the origin of enantioselectivity. We already used the steric maps to rationalize the behavior of Ru complexes active in olefins metathesis.[21]

The topographic steric maps can be considered as the classical geographic physical maps, that depict the physical features like various landforms and water bodies present on the Earth's surface. Different colors, lines, tints, shading and spot elevations are used to show the elevation and to differentiate lowlands from the mountains in physical maps. We used the same philosophy to build the steric maps of both L-**1** and L-**2**. The Rh center is at level zero, and the ligand is placed below the metal, as in the scheme of Figure 1 and the structures of Figure 3. The substrates approach the metal from the top, again as in Figures 1 and 3. In this framework, brown areas indicate zones where the ligand protrudes like a mountain towards the reacting groups, thus limiting the space at their disposal, whereas blue areas indicate empty zones where the ligand retracts like a lake from the reacting groups. In this specific case, the steric maps have been calculated for one unit of the dimeric $[$L-**1**RhCl$]_2$ and $[$L-**2**RhCl$]_2$ precursors of L-**1** and L-**2**, optimized under a C_2-symmetric constraint. The topographic electrostatic maps were obtained through a representation of the electrostatic potentials calculated in the points defining the topographic steric maps. The electrostatic maps clarify which is the electrostatic situation at the surface defining the catalyst–substrate interaction. In the frame of the induced fit model developed for enzymatic catalysis, specificity (enantioselectivity in this case) is determined by which prochiral enantioface of the substrate complements better with the catalyst shape. This specificity can be analyzed using topographic steric and electrostatic maps.

Focusing first on the steric maps, that of the ligand of L-**1** (see Figure 4a), is rather flat, with negligible steric pale brown/orange hills around the S=O bonds in the top-right and bottom-left quadrants, and shallow green valleys around the pointing down phenyl groups of the ligand in the top-left and bottom-right quadrants. Differently, the steric map

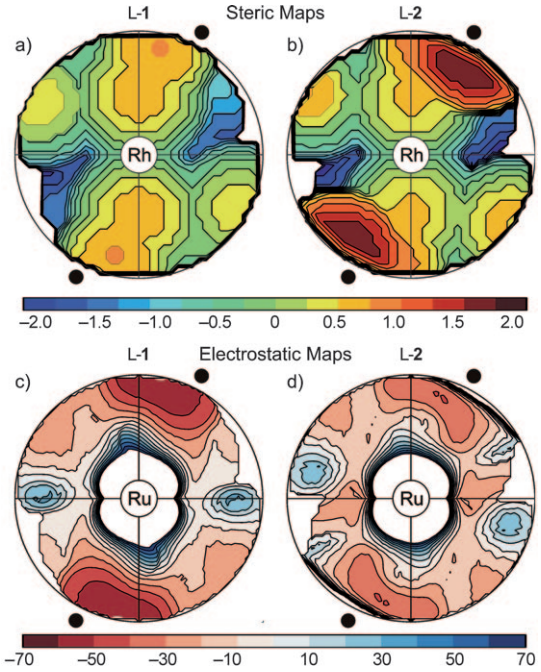

Figure 4. Topographic steric (a and b) and electrostatic potential (c and d) maps for L-**1** and L-**2**. The isocontor energy curves of the steric and electrostatic potential maps are in Å and kcal mol^{-1}, respectively. The orientation of the ligands is identical to that in Figure 3. That is, the ligands develop beneath the sheet, and the small black circles indicate the quadrants occupied by the S=O groups in L-**1** and the pointing up *p*-tolyl groups in L-**2**.

of the ligand of L-**2** (see Figure 4b), presents brown colored high protuberances in the correspondence of the phenyl groups of the ligand that are pointing up, in the top-right and bottom-left quadrants, while green/orange colored flat valleys correspond to the phenyl groups of the ligand that are pointing down in the top-left and bottom-right quadrants. This clearly indicates that the pointing up phenyl groups in L-**2** shape sterically a highly C_2-symmetric chiral pocket, where the pro-*R* transition state fits well, while the pro-*S* transition state is bumping onto the steric hills. Differently, in L-**1** the S=O groups have a negligible steric influence in the first coordination sphere of the metal, which indicates that the origin of stereoselectivity in L-**1** cannot be ascribed to a steric influence of these groups. Moving to the electrostatic maps, reporting the electrostatic potential calculated at the same points defining the corresponding steric map, the situation of L-**1** and L-**2** is completely reversed. In fact, the electrostatic map of L-**1** presents zones of strongly negative electrostatic potential, evidenced by the deep red zones around the pointing up S=O groups in Figure 4c. This clearly indicates that the pointing up S=O groups in L-**1** shape electrostatically a highly C_2-symmetric chiral pocket, where the pro-*R* transition state fits well, while the pro-*S* transition state is repulsively interacting with the electrostatic hills. Again, the map of L-**2** is totally different, and in this case is rather flat (Figure 4d), with no appreciable difference between the zones corresponding to the pointing down and to the pointing up phenyl groups of the ligand. This indicates that both the pro-*R* and pro-*S* transition states fit well in the first coordination sphere of the metal in L-**2**, when its first coordination sphere is analysed in terms of electrostatic effects.

The comparative analysis of L-**1** and L-**2** in terms of steric and electrostatic topographic maps indicates that the same enantioselective induction can be obtained by using the same basic skeleton, corresponding to a square-planar Rh complex, but storing the chiral information with either steric or electrostatic effects. In both catalytic systems, the atropisomeric backbone orients the groups ultimately responsible for enantioselectivity in such a way as to discriminate between the possible pathways that lead to the enantiomerically enriched product of the reaction.[37] This interchange between these effects is striking, and indicates possible directions for the development of better performing catalytic systems as the focus of chemistry is shifting from molecular structure to molecular function.[38] It is probably a weakness of our classification schemes that have induced to privilege more the easy to understand and quantify steric handle relative to the more complex electrostatic counterpart.

On the other hand, we believe that topographic steric and electrostatic potential maps as those shown in Figure 4 could help to analyze rapidly a given catalyst, and could even help to rationally design catalysts where steric and electrostatic effects are modulated to achieve the desired performances. This conclusion is also in line with extremely recent work providing a view of nonbonded interactions as continuous surfaces rather than close contacts between atom pairs.[39] Interestingly, also the authors of this paper argued that the analysis of the surface of interaction can offer rich insight into the design of new and improved ligands.

As a final remark, we stress that the topographic steric and electrostatic maps have been calculated using the optimized structure of the simple (pre)catalyst, which means in the absence of any reacting group. This is potentially very useful, since this kind of analysis is computationally fast and could allow to screen rapidly the impact that a large number of modifications/substitutions of a parent ligand structure have on the first coordination sphere of the metal, steering experimental efforts towards the most promising solutions. Controlling this point is at the basis of the rational catalysts design.

Conclusion

In this paper we provide evidence on how high enantioselectivity in transition-metal-promoted asymmetric synthesis can be achieved using either steric or electrostatic effects to shape a chiral pocket around the metal centre. To clarify this point we compared two strictly related square-planar chiral Rh catalysts active in the asymmetric 1,4-addition of phenylboronic acid to 2-cyclohexenone leading to chiral 3-phenylcyclohexanone. We first performed static DFT calculations that indicated that the rate-determining enantioselec-

tive step corresponds to the transition state for C–C bond formation. However, these calculations simply indicate that, in agreement with the experimental results, the two chiral Rh catalysts are able to differentiate between the two prochiral faces of the cyclohexenone substrate. To really demonstrate the origin of this selectivity we took advantage of steric and electrostatic topographic maps that clearly illuminated that in one case, L-**2**, selection between the two prochiral faces of the cyclohexenone is due to steric effects only (nearly flat electrostatic map combined with a strongly asymmetric steric map), while in the other case, L-**1**, selection is due to electrostatic effects only (nearly flat steric map combined with a strongly asymmetric electrostatic map). Of course, our analysis does not exclude that both effects could be present in other catalysts, and actually the experimental behavior of a given catalyst always is the result of both effects.

We believe our results reinforce the general idea that electrostatic effects have a great potential in the rational design of new catalysts, possibly in synergy with the well-controlled steric handle. This rational design could be also sped up by checking the effects of ligands modification on the first coordination sphere of the metal using steric and/or electrostatic maps. These checks could be done before the time and money consuming synthesis of an ineffective catalyst.

Acknowledgements

R.D. holds an Alfred Werner Assistant Professorship and thanks the foundation for generous financial support. R.M. thanks the Swiss National Science Foundation (SNF) for support. A.P. is grateful for the allocation of a Ramón y Cajal contract by the Spanish MICINN. We thank the HPC team of Enea (http://www.enea.it) for using the ENEA-GRID and the HPC facilities CRESCO (http://www.cresco.enea.it) in Portici, Italy.

[1] G. Natta in *Nobel Lectures in Chemistry 1963–1970*, Elsevier, Amsterdam, **1972**, p. 27.
[2] J. A. Gladysz, *Chem. Rev.* **2000**, *100*, 1167.
[3] W. S. Knowles, *Angew. Chem.* **2002**, *114*, 2096; *Angew. Chem. Int. Ed.* **2002**, *41*, 1998.
[4] R. Noyori, *Angew. Chem.* **2002**, *114*, 2108; *Angew. Chem. Int. Ed.* **2002**, *41*, 2008.
[5] J. Christoffers, G. Koripelly, A. Rosiak, M. Rössle, *Synthesis* **2007**, 1279.
[6] B. L. Feringa, M. Pineschi, L. A. Arnold, R. Imbos, A. H. M. d. Vries, *Angew. Chem.* **1997**, *109*, 2733; *Angew. Chem. Int. Ed. Engl.* **1997**, *36*, 2620.
[7] B. M. Trost, M. L. Crawley, *Chem. Rev.* **2003**, *103*, 2921.
[8] D. A. Evans, J. Bartroli, T. L. Shih, *J. Am. Chem. Soc.* **1981**, *103*, 2127.
[9] R. Bentley, *Nature* **1978**, *276*, 673.
[10] A. G. Ogston, *Nature* **1978**, *276*, 676.
[11] B. Honig, A. Nicholls, *Science* **1995**, *268*, 1144.
[12] A. C. R. Martin, J. M. Thornton, *J. Mol. Biol.* **1996**, *263*, 800.
[13] Y.-D. Wu, D. K. W. Lai, *J. Am. Chem. Soc.* **1995**, *117*, 11327.
[14] K. A. Joergensen, R. A. Wheeler, R. Hoffmann, *J. Am. Chem. Soc.* **1987**, *109*, 3240.
[15] Y. Gao, J. M. Klunder, R. M. Hanson, H. Masamune, S. Y. Ko, K. B. Sharpless, *J. Am. Chem. Soc.* **1987**, *109*, 5765.
[16] T. Hayashi, K. Yamasaki, *Chem. Rev.* **2003**, *103*, 2829.
[17] T. Korenaga, K. Osaki, R. Maenishi, T. Sakai, *Org. Lett.* **2009**, *11*, 2325.
[18] J. J. Bürgi, R. Mariz, M. Gatti, E. Drinkel, X. Luan, S. Blumentritt, A. Linden, R. Dorta, *Angew. Chem.* **2009**, *121*, 2806; *Angew. Chem. Int. Ed.* **2009**, *48*, 2768.
[19] R. Mariz, A. Poater, M. Gatti, E. Drinkel, J. J. Bürgi, X. Luan, S. Blumentritt, A. Linden, L. Cavallo, R. Dorta, *Chem. Eur. J.* **2010**, *16*, 14335.
[20] C. Costabile, L. Cavallo, *J. Am. Chem. Soc.* **2004**, *126*, 9592.
[21] F. Ragone, A. Poater, L. Cavallo, *J. Am. Chem. Soc.* **2010**, *132*, 4249.
[22] Gaussian 03, Revision B.1, M. J. Frisch, G. W. Trucks, H. B. Schlegel, G. E. Scuseria, M. A. Robb, J. R. Cheeseman, J. Montgomery, Jr., J. A., T. Vreven, K. N. Kudin, J. C. Burant, J. M. Millam, S. S. Iyengar, J. Tomasi, V. Barone, B. Mennucci, M. Cossi, G. Scalmani, N. Rega, G. A. Petersson, H. Nakatsuji, M. Hada, M. Ehara, K. Toyota, R. Fukuda, J. Hasegawa, M. Ishida, T. Nakajima, Y. Honda, O. Kitao, H. Nakai, M. Klene, X. Li, J. E. Knox, H. P. Hratchian, J. B. Cross, C. Adamo, J. Jaramillo, R. Gomperts, R. E. Stratmann, O. Yazyev, A. J. Austin, R. Cammi, C. Pomelli, J. W. Ochterski, P. Y. Ayala, K. Morokuma, G. A. Voth, P. Salvador, J. J. Dannenberg, V. G. Zakrzewski, S. Dapprich, A. D. Daniels, M. C. Strain, O. Farkas, D. K. Malick, A. D. Rabuck, K. Raghavachari, J. B. Foresman, J. V. Ortiz, Q. Cui, A. G. Baboul, S. Clifford, J. Cioslowski, B. B. Stefanov, G. Liu, A. Liashenko, P. Piskorz, I. Komaromi, R. L. Martin, D. J. Fox, T. Keith, M. A. Al-Laham, C. Y. Peng, A. Nanayakkara, M. Challacombe, P. M. W. Gill, B. Johnson, W. Chen, M. W. Wong, C. Gonzalez, J. A. Pople, Gaussian, Inc., Pittsburgh PA, **2003**.
[23] A. D. Becke, *Phys. Rev. A* **1988**, *38*, 3098.
[24] J. P. Perdew, *Phys. Rev. B* **1986**, *34*, 7406.
[25] J. P. Perdew, *Phys. Rev. B* **1986**, *33*, 8822.
[26] F. Weigend, R. Ahlrichs, *Phys. Chem. Chem. Phys.* **2005**, *7*, 3297.
[27] J. Tomasi, B. Mennucci, R. Cammi, *Chem. Rev.* **2005**, *105*, 2999.
[28] A. Poater, B. Cosenza, A. Correa, S. Giudice, F. Ragone, V. Scarano, L. Cavallo, *Eur. J. Inorg. Chem.* **2009**, 1759.
[29] L. Cavallo, A. Correa, C. Costabile, H. Jacobsen, *J. Organomet. Chem.* **2005**, *690*, 5407.
[30] A. Poater, F. Ragone, S. Giudice, C. Costabile, R. Dorta, S. P. Nolan, L. Cavallo, *Organometallics* **2008**, *27*, 2679.
[31] A. Poater, L. Cavallo, *Dalton Trans.* **2009**, 8878.
[32] H. Jacobsen, A. Correa, A. Poater, C. Costabile, L. Cavallo, *Coord. Chem. Rev.* **2009**, *253*, 687.
[33] X. Luan, R. Mariz, M. Gatti, C. Costabile, A. Poater, L. Cavallo, A. Linden, R. Dorta, *J. Am. Chem. Soc.* **2008**, *130*, 6848.
[34] J. Bosson, A. Poater, L. Cavallo, S. P. Nolan, *J. Am. Chem. Soc.* **2010**, *132*, 13146.
[35] A. Bondi, *J. Phys. Chem.* **1964**, *68*, 441.
[36] Y. Takaya, M. Ogasawara, T. Hayashi, M. Sakai, N. Miyaura, *J. Am. Chem. Soc.* **1998**, *120*, 5579.
[37] Recent results by Liao et al. have shown that chiral sulfoxide ligands that do not incorporate an additional element of chirality (atropisomeric backbone) can also be used to good effect in the rhodium-catalyzed 1,4-addition reaction, see: a) F. Lang, D. Li, J. Chen, J. Chen, L. Li, L. Cun, J. Zhu, J. Deng, J. Liao, *Adv. Synth. Catal.* **2010**, *352*, 843; b) J. Chen, J. Chen, F. Lang, X. Zhang, L. Cun, J. Zhu, J. Deng, J. Liao, *J. Am. Chem. Soc.* **2010**, *132*, 4552.
[38] X. Wu, P. G. Schultz, *J. Am. Chem. Soc.* **2009**, *131*, 12497.
[39] E. R. Johnson, S. Keinan, P. Mori-Sánchez, J. Contreras-García, A. J. Cohen, W. Yang, *J. Am. Chem. Soc.* **2010**, *132*, 6498.

Received: July 8, 2010
Revised: September 18, 2010
Published online: November 16, 2010

